
Hyperbolic Embedding Inference for Structured Multi-Label Prediction

Bo Xiong*
University of Stuttgart
Stuttgart, Germany

Michael Cochez
Vrije Universiteit Amsterdam
Discovery Lab, Elsevier
Amsterdam, The Netherlands

Mojtaba Nayyeri
University of Stuttgart
Stuttgart, Germany

Steffen Staab
University of Stuttgart
University of Southampton
Stuttgart, Germany

Abstract

We consider a structured multi-label prediction problem where the labels are organized under implication and mutual exclusion constraints. A major concern is to produce predictions that are logically consistent with these constraints. To do so, we formulate this problem as an *embedding inference* problem where the constraints are imposed onto the embeddings of labels by *geometric construction*. Particularly, we consider a hyperbolic Poincaré ball model in which we encode labels as Poincaré hyperplanes that work as linear decision boundaries. The hyperplanes are interpreted as convex regions such that the logical relationships (implication and exclusion) are geometrically encoded using *insideness* and *disjointedness* of these regions, respectively. We show theoretical groundings of the method for preserving logical relationships in the embedding space. Extensive experiments on 12 datasets show 1) significant improvements in mean average precision; 2) lower number of constraint violations; 3) an order of magnitude fewer dimensions than baselines.

1 Introduction

Structured multi-label prediction is a task aiming to associate every object with multiple labels that are semantically constrained in a structured manner (e.g., by implication and exclusion constraints). This task is of growing importance in many applications such as image annotation [1, 2], text categorization [3, 4] and functional genomics [5, 6]. One of the central concerns of the task is to produce predictions that are *logically consistent* with the constraints of the labels. For example, a protein must be labeled to have the function *nucleic acid binding* if it is already labeled to have the function *RNA binding* (i.e., implication) and must not have the function *drug binding* (i.e., mutual exclusion).

Various works have been proposed to improve the prediction consistency [7, 8, 9, 10, 11]. One line of work called *label embedding* aims to represent labels as low-dimensional vectors [12, 13]. A key disadvantage of the vector-based representations is that they only capture weak forms of correlation or “similarity” between labels, but do not strongly enforce the logical relationships. Another line of work [7, 9, 14, 8] imposes these logical constraints directly to the losses of neural networks. However, they do not explicitly learn the representations of labels and typically require a complete label taxonomy, which is not always available in and scalable to real-world settings [11].

*Correspondence to bo.xiong@ipvs.uni-stuttgart.de

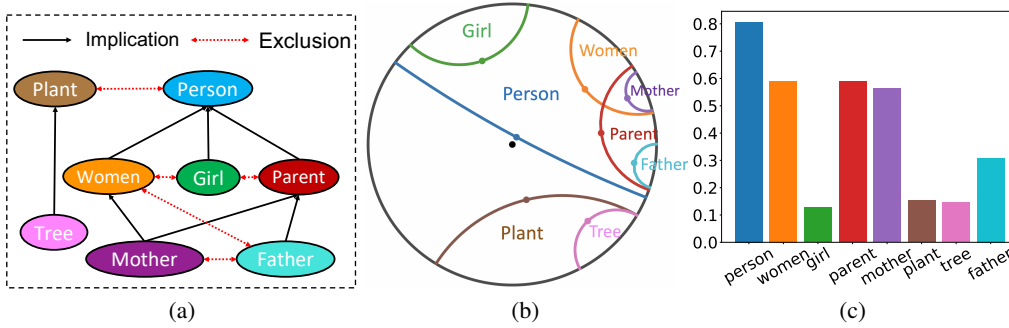


Figure 1: (a) A HEX graph describing the logical relationships (implication and exclusion) between different labels; (b) The learned label embeddings (linear decision boundaries) in the Poincaré ball, where all constraints in the HEX graph are respected; (c) The prediction scores of a given instance of *mother* respect all constraints in the HEX graph, where each score is calculated as the confidence of the instance embedding being a member of the convex region of the corresponding label embedding.

Embedding-based inference [15], which imposes logical constraints directly to the label embeddings, is able to *inductively* infer the underlying label relationships from incomplete labelings [16]. Once all embeddings are adhering to the constraints, each label can be predicted independently without accessing the label relationships, which significantly reduces the computation cost during inference [15]. The key idea, which is inspired by the Venn diagram [16, 17] or set-theoretic semantics [18], is to represent each label as a convex region [15]. A prominent example is the multi-label box model (MBM) [11] that models label implications as box containments. However, MBM learns box-like decision boundaries, which are typically not compatible with standard classifiers (i.e., hyperplane margin-based models such as logistic regression [19]). Besides, box models suffer from a theoretical limitation, i.e., lower-way intersections enforce higher-way interactions [20]. Finally, current methods ignore the importance of constraining mutual exclusion, which is essential as otherwise, a model could trivially obtain zero implication violation by assigning the same score to all labels.

In this paper, we consider a structured multi-label prediction problem with *implication* and *mutual exclusion* constraints that are jointly described by a hierarchy and exclusion (HEX) graph (see Figure 1(a) for an example). The key idea of our method is to transform the logical constraints into soft geometric constraints in the embedding space. In particular, we consider a hyperbolic Poincaré ball model that has demonstrated advantages in representing hierarchies and assign each label a Poincaré hyperplane that has several favorable theoretical properties in classification. Each Poincaré hyperplane can be interpreted as a convex region such that the *implication* and *mutual exclusion* are modeled by geometric *insideness* and *disjointness* between the corresponding regions, respectively. In this way, a multi-label classifier can be defined by measuring the confidence of an instance having a label as geometric *membership*. Unlike other hyperbolic region-based models such as hyperbolic cones [21] and hyperbolic disks [22], Poincaré hyperplane works as a linear decision boundary and can be seamlessly integrated into existing margin-based classifiers such as hyperbolic logistic regression [19]. Figure 1(b) shows an example of the learned label representations that respect all the constraints given in Figure 1(a). We show theoretical groundings of the proposed method on modeling *implication* and *mutual exclusion*. Extensive experiments on 12 multi-label classification tasks show the model’s capability to improve the mean average precision significantly while keeping the number of constraint violations low and requiring an order of magnitude fewer dimensions.

2 Preliminaries

Poincaré ball model The Poincaré ball ($\mathbb{D}^n, g^{\mathbb{D}}$) is one of the models of hyperbolic geometry that is very suitable for representing hierarchies due to its exponentially growing volume [23]. The Poincaré ball is defined as an open n -ball $\mathbb{D}^n = \{\mathbf{x} \in \mathbb{R}^n : \|\mathbf{x}\| < 1\}$ equipped with a Riemannian metric $g_{\mathbf{x}}^{\mathbb{D}} = \lambda_{\mathbf{x}}^2 g^E$, where $\lambda_{\mathbf{x}} = \frac{2}{1-\|\mathbf{x}\|^2}$, $g^E = \mathbf{I}_n$ is the Euclidean metric tensor, $\lambda_{\mathbf{x}}$ is the *conformal factor*, and $\|\cdot\|^2$ denotes the L^2 norm in Euclidean space. The distance between two points $\mathbf{x}, \mathbf{y} \in \mathbb{D}^n$ can be defined by $d_{\mathbb{D}}(\mathbf{x}, \mathbf{y}) = \cosh^{-1} \left(1 + 2 \frac{\|\mathbf{x} - \mathbf{y}\|^2}{(1-\|\mathbf{x}\|^2)(1-\|\mathbf{y}\|^2)} \right)$.

Structured multi-label prediction Let $\mathcal{X} \subseteq \mathbb{R}^n$ denote an n -dimensional instance space and $\mathcal{L} = \{l_1, l_2, \dots\}$, $|\mathcal{L}| \geq 2$ denote the finite set of possible labels. Given a set of N training examples $\mathcal{D} = \{(x_i, L_i) \mid 1 \leq i \leq N, x_i \in \mathcal{X}, L_i \subset \mathcal{L}\}$, *multi-label prediction* aims to learn a labeling function $f : \mathcal{X} \rightarrow 2^{\mathcal{L}}$ mapping from the instance space to the powerset of the label space, $f(x) \subset \mathcal{L}$.

Structured multi-label prediction additionally imposes a set of prior-known logical constraints over the labels, namely, the predictions must be logically consistent with these constraints. Analogous to Mirzazadeh et al. [15], we consider two forms of logical constraints between labels: implication and mutual exclusion. Specifically, an *implication* of the form $l_a \Rightarrow l_b$ imposes the constraint that whenever an instance is labeled as l_a then it must also be labeled as l_b , i.e., $l_a \Rightarrow l_b$ is a shorthand notation for $\forall x \in \mathcal{X}, l_a \in f(x) \Rightarrow l_b \in f(x)$. *Mutual exclusions* are constraints of the form $\neg l_a \vee \neg l_b$, implying that an instance cannot be simultaneously labeled as l_a and l_b , i.e., $\neg l_a \vee \neg l_b$ is a shorthand notation for $\forall x \in \mathcal{X}, l_a \notin f(x) \vee l_b \notin f(x)$. We can concisely represent a set of implication and exclusion constraints with a hierarchy and exclusion (HEX) graph [2].

Definition 1 (HEX graph [2]²). A *HEX graph* $G = (V, E_h, E_e)$ is a graph consisting of a set of nodes $V = \{v_1, \dots, v_n\}$, directed (hierarchy) edges $E_h \subseteq V \times V$, and undirected (exclusion) edges $E_e \subseteq V \times V$, such that the subgraph $G_h = (V, E_h)$ is a DAG and the subgraph $G_e = (V, E_e)$ has no self loop. Each node $v_i \in V$ represents the label l_i . A directed edge $(v_i, v_j) \in E_h$ represents the implication $l_i \Rightarrow l_j$, and an undirected edge $(v_i, v_j) \in E_e$ represents the exclusion $\neg l_i \vee \neg l_j$.

Note that an arbitrary HEX graph may contain redundant edges. A hierarchy edge (v_i, v_j) is redundant when there is a path in G_h from v_i to v_j which does not contain the edge (v_i, v_j) . Similarly, an exclusion edge (v_i, v_j) is redundant when there is another exclusion edge connecting their ancestors (or connecting one node's ancestor to the other node). We can transform a HEX graph into an equivalent HEX graph by adding or removing redundant edges. In this paper, we only consider HEX graphs that have a minimal number of edges, we call such HEX graph a *minimal sparse* HEX graph (see Fig. 1(a) for an example). Given a minimal sparse HEX graph, we define the HEX-property as

Definition 2 (HEX-property). A labeling function f has the *HEX property* with respect to a HEX graph G if for all $x \in \mathcal{X}$, $f(x)$ respects all constraints represented by G .

We also call such function f *logically consistent* w.r.t G . Given the HEX graph and the HEX-property, structured multi-label prediction is formally defined as a constrained optimization problem.

Definition 3 (Structured multi-label prediction). The *structured multi-label prediction task* with respect to a training set $\mathcal{D} = \{(x_i, L_i) \mid 1 \leq i \leq N, x_i \in \mathcal{X}, L_i \subset \mathcal{L}\}$, minimal HEX graph $G = (V, E_h, E_e)$, and multi-label prediction function f , is the task of learning f such that the function f minimizes $\sum_{(x_i, L_i) \in \mathcal{D}} \text{loss}(f(x_i), L_i)$, with loss a predefined function, while attempting to maintain the HEX-property with respect to G .

Note that this definition allows for a *soft* interpretation of the constraints, meaning that the goal is to adhere to all of them, but we do allow for loosening some if necessary. For example, a mutual exclusion constraint is allowed to loosen when an instance (e.g., image), though rarely happens, is simultaneously labeled as two mutual exclusive labels (e.g., *dog* and *cat*).

3 Hyperbolic embedding inference

We consider learning a real-valued ranking function $h : \mathcal{X} \times \mathcal{L} \mapsto [0, 1]$, where the output is interpreted as the confidence of an instance $x \in \mathcal{X}$ having a label $l \in \mathcal{L}$. Afterward, a binary multi-label classifier $f : \mathcal{X} \rightarrow 2^{\mathcal{L}}$ can be simply obtained by thresholding the ranking function with a threshold t , i.e., $f(x) = \{l \mid h(x, l) \geq t, \forall l \in \mathcal{L}\}$. The objective of h is to assign higher scores to positive instance-label pairs than that of negative instance-label pairs.

3.1 Geometric construction

Given an n -dimensional Poincaré ball \mathbb{D}^n , we associate each instance $x_i \in \mathcal{X}$ with a point in the Poincaré ball and associate each label $l_i \in \mathcal{L}$ with a Poincaré hyperplane, such that its corresponding positive and negative instances are correctly separated by the hyperplane.

²Deng et al. [2] use subsumption, which is the inverse relation of implication that we use here.

Poincaré hyperplanes Let \mathbb{B}^n denote the set of n -balls in \mathbb{R}^n whose boundaries $\partial\mathbb{B}^n$ intersect the Poincaré ball \mathbb{D}^n perpendicularly. Poincaré hyperplanes are defined by $\partial\mathbb{B}^n \cap \mathbb{D}^n$ (see Fig. 2(a)) plus all linear subspaces going through the origin. For the former cases, a Poincaré hyperplane can be uniquely defined by its center point that has a minimal distance to the origin.

Definition 4. Given a (center) point $\mathbf{c} \in \mathbb{D}^n$ where $\mathbf{c} \neq \mathbf{0}$, the Poincaré hyperplane is defined as

$$H_{\mathbf{c}} = \{\mathbf{p} \in \mathbb{D}^n : g^{\mathbb{D}}(\log_{\mathbf{c}}(\mathbf{p}), \vec{\mathbf{c}}) = 0\} \quad (1)$$

where \mathbf{c} is the center point and $\vec{\mathbf{c}} \in T_{\mathbf{c}}\mathbb{D}^n$ ³ is the normal vector passing through the origin $\mathbf{0}$.

Intuitively, this corresponds to the union of all geodesics passing through \mathbf{c} while orthogonal to the normal vector $\vec{\mathbf{c}} \in T_{\mathbf{c}}\mathbb{D}^n$. In the case where \mathbf{c} is the center of the hyperplane, $\vec{\mathbf{c}}$ must simultaneously pass through \mathbf{c} and the origin. Hence, $\vec{\mathbf{c}}$ can be simply taken as \mathbf{c} without loss of generality. For the special case where $\mathbf{c} = \mathbf{0}$, the Poincaré hyperplanes are all linear subspaces (Euclidean planes) passing through the origin. In this paper, we exclude these special cases by assuming $\mathbf{c} \neq \mathbf{0}$.

Geometric intuition Essentially, the Poincaré hyperplane works as a linear decision boundary that separates the embedding space into two regions,⁴ where the smaller region (i.e., convex hull) is interpreted as the space of positive samples while the other one is interpreted as the space of negative samples. Two reasons motivate us to model labels as Poincaré hyperplanes: 1) Modeling labels as hyperplanes has several desired theoretical advantages in margin-based classifiers. Our model shares the same philosophy as existing learning frameworks such as hyperbolic logistic regression [19] and hyperbolic SVM [24]; 2) More importantly, unlike Euclidean space that is flat, hyperbolic Poincaré ball is a curved space in which there are infinitely many non-parallel hyperplanes which do not intersect, implying that linear decision boundaries in hyperbolic space can capture more complicated set-theoretic interactions, such as implication and mutual exclusion.

Enclosing balls Given a Poincaré hyperplane $H_{\mathbf{c}}$, we call the corresponding n -ball $\mathbb{B}_{\mathbf{c}}^n$ that encloses $H_{\mathbf{c}}$ its enclosing n -ball. Formally, an enclosing n -ball $\mathbb{B}^n(\mathbf{o}, r)$ is defined by $\mathbb{B}^n(\mathbf{o}, r) = \{\mathbf{p} : \|\mathbf{p} - \mathbf{o}\| \leq r\}$, where $\mathbf{o} \in \mathbb{R}^n$ and r are the center point and the radius, respectively. Given $H_{\mathbf{c}}$, we have the following closed-form representation of $\mathbb{B}_{\mathbf{c}}^n$.

Proposition 1. Given a Poincaré hyperplane $H_{\mathbf{c}}$ where $\mathbf{c} \neq \mathbf{0}$, there exists an n -ball $\mathbb{B}_{\mathbf{c}}^n(\mathbf{o}_{\mathbf{c}}, r_{\mathbf{c}})$ such that $H_{\mathbf{c}} \subset \mathbb{B}_{\mathbf{c}}^n(\mathbf{o}_{\mathbf{c}}, r_{\mathbf{c}})$, i.e., $H_{\mathbf{c}}$ is a subset of $\mathbb{B}_{\mathbf{c}}^n(\mathbf{o}_{\mathbf{c}}, r_{\mathbf{c}})$. $\mathbb{B}_{\mathbf{c}}^n$ is uniquely given by

$$\mathbb{B}_{\mathbf{c}}^n = \mathbb{B}^n\left(\frac{(1 + \|\mathbf{c}\|^2)}{2\|\mathbf{c}\|}\mathbf{c}, \frac{1 - \|\mathbf{c}\|^2}{2\|\mathbf{c}\|}\right) \quad (2)$$

Proof sketch. The key idea is to solve a quadratic equation given by the fact that the radius of $\mathbb{B}_{\mathbf{c}}^n$, the radius of \mathbb{D}^n , and the distance from the center of \mathbb{D}^n to the center of $\mathbb{B}_{\mathbf{c}}^n$ must satisfy the Pythagorean theorem [25]. Full proof is in the supplementary material.

3.2 Geometric interpretation

Our main idea is to transform the logical relationships between labels into geometric relationships between their corresponding enclosing n -balls. In particular, the implication is modeled by the geometric insideness while the mutual exclusion is modeled by the geometric disjointness.

Implication The logical implication between two labels is interpreted as geometric relations between n -balls, i.e., n -ball insideness illustrated in Fig. 2(b). In particular, an n -ball $\mathbb{B}_{\mathbf{w}}(\mathbf{o}_{\mathbf{w}}, r_{\mathbf{w}})$ contains $\mathbb{B}_{\mathbf{u}}(\mathbf{o}_{\mathbf{u}}, r_{\mathbf{u}})$ if and only if $\|\mathbf{o}_{\mathbf{u}} - \mathbf{o}_{\mathbf{w}}\| + r_{\mathbf{u}} < r_{\mathbf{w}}$, and thus we can create an insideness loss defined by

$$\mathcal{L}_{\text{inside}}(\mathbb{B}_{\mathbf{u}}, \mathbb{B}_{\mathbf{w}}) = \max\{0, \|\mathbf{o}_{\mathbf{u}} - \mathbf{o}_{\mathbf{w}}\| + r_{\mathbf{u}} - r_{\mathbf{w}}\}. \quad (3)$$

Clearly, the insideness loss term satisfies the properties of correctness and transitivity

Lemma 1 (Correctness). $\mathbb{B}_{\mathbf{u}}$ is inside of $\mathbb{B}_{\mathbf{w}}$ if and only if $\mathcal{L}_{\text{inside}}(\mathbb{B}_{\mathbf{u}}, \mathbb{B}_{\mathbf{w}}) = 0$.

Lemma 2 (Transitivity). If $\mathcal{L}_{\text{inside}}(\mathbb{B}_{\mathbf{u}}, \mathbb{B}_{\mathbf{w}}) = 0$ and $\mathcal{L}_{\text{inside}}(\mathbb{B}_{\mathbf{w}}, \mathbb{B}_{\mathbf{v}}) = 0$, we have $\mathcal{L}_{\text{inside}}(\mathbb{B}_{\mathbf{u}}, \mathbb{B}_{\mathbf{v}}) \leq \mathcal{L}_{\text{inside}}(\mathbb{B}_{\mathbf{u}}, \mathbb{B}_{\mathbf{w}}) + \mathcal{L}_{\text{inside}}(\mathbb{B}_{\mathbf{w}}, \mathbb{B}_{\mathbf{v}}) \leq \mathcal{L}_{\text{inside}}(\mathbb{B}_{\mathbf{w}}, \mathbb{B}_{\mathbf{v}}) = 0$.

³In this paper, we distinguish normal vectors from regular points by adding an arrow on top of its letters.

⁴Note that by using the metric in the Poincaré ball, each region has infinite (exponentially growing) volume.

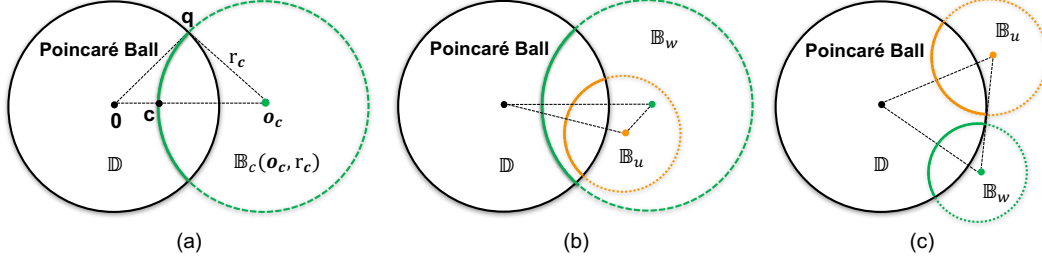


Figure 2: (a) A Poincaré hyperplane is defined as the intersection between the Poincaré ball \mathbb{D} and the boundary of an n -ball \mathbb{B}_c . The Poincaré hyperplane is uniquely parameterized by a center point \mathbf{c} , and the corresponding n -ball (its radius and center) can be uniquely determined by Proposition 1. (b) Label implication is interpreted as n -ball insideness. (c) Mutual exclusion is interpreted as n -ball disjointedness.

Mutual exclusion Similarly, we interpret mutual exclusion as geometric disconnectedness between n -balls illustrated in Fig. 2(c). \mathbb{B}_u disconnecting from \mathbb{B}_w can be measured by subtracting the distance between their center points from the sum of their radii. Inversely, the corresponding loss is

$$\mathcal{L}_{\text{disjoint}}(\mathbb{B}_u, \mathbb{B}_w) = \max\{0, r_w + r_u - \|\mathbf{o}_u - \mathbf{o}_w\|\} \quad (4)$$

Again, the disjointedness loss term satisfies the correctness property

Lemma 3 (Correctness). \mathbb{B}_u disconnects from \mathbb{B}_w if and only if $\mathcal{L}_{\text{disjoint}}(\mathbb{B}_u, \mathbb{B}_w) = 0$.

3.3 Classification and learning

Given the embeddings of instances and labels, an instance can be classified by measuring the *geometric membership*, i.e., the confidence of a point $\mathbf{p} \in \mathbb{D}^n$ being inside the enclosing ball \mathbb{B} .

Membership and non-membership Formally, given an instance embedding $\mathbf{p} \in \mathbb{D}^n$ and a label embedding associated with an enclosing n -ball \mathbb{B}_c . The confidence of an instance \mathbf{p} being inside the enclosing n -ball \mathbb{B}_c can be measured by subtracting the distance between the center point of \mathbb{B}_c and \mathbf{p} from the radius of \mathbb{B}_c . The corresponding loss is defined as the inverse of the measure, given by

$$\mathcal{L}_{\text{membership}}(\mathbf{p}, \mathbb{B}_c(\mathbf{o}_c, r_c)) = \max\{0, \|\mathbf{o}_c - \mathbf{p}\| - r_c\}. \quad (5)$$

Symmetrically, for negative instance-label relations, the loss of non-membership can be defined as

$$\mathcal{L}_{\text{non-membership}}(\mathbf{p}, \mathbb{B}_c(\mathbf{o}_c, r_c)) = \max\{0, r_c - \|\mathbf{o}_c - \mathbf{p}\|\}. \quad (6)$$

Clearly, we have the following properties that follow directly from the definitions.

Lemma 4. A point \mathbf{p} is a member of \mathbb{B}_c if and only if $\mathcal{L}_{\text{membership}}(\mathbf{p}, \mathbb{B}_c) = 0$.

Lemma 5. A point \mathbf{p} is not a member of \mathbb{B}_c if and only if $\mathcal{L}_{\text{non-membership}}(\mathbf{p}, \mathbb{B}_c) = 0$.

Lemma 1-2, Lemma 3, Lemma 4-5 immediately follow the definitions of geometric insideness, disjointedness, and membership, respectively.

We aim to learn an encoder E_θ (i.e., a hyperbolic neural network whose designs depend on the datasets), where θ is the trainable parameter, and a function \mathcal{C} which maps labels to the center points of the corresponding Poincaré hyperplanes in the Poincaré ball.

Now, we define $h(x, l) = \sigma(\mathcal{L}_{\text{non-membership}}(E_\theta(x), \mathcal{C}(l)) - \mathcal{L}_{\text{membership}}(E_\theta(x), \mathcal{C}(l)))$, as our ranking function, where σ is the sigmoid function. The final classification function is then defined by $f(x) = \{l \mid h(x, l) \geq 0.5\}$. We call our classifier *hyperbolic multi-label embedding inference* (HMI). Given a HEX graph, HMI has the following guarantee.

Proposition 2 (HEX-property). *The classification function f of HMI has the HEX property with respect to G if for any constraint in G , the corresponding loss term is 0.*

Learning with soft constraints Let $\mathcal{D}^+ = \{(x_i, l_n) \mid (x_i, L_i) \in \mathcal{D}, l_n \in L_i\}$ be the set of positive instance-label pairs and $\mathcal{D}^- = \{(x_i, l_n) \mid (x_i, L_i) \in \mathcal{D}, l_n \in \mathcal{L}, l_n \notin L_i\}$ be the set of negative instance-label pairs. By combining the loss functions of membership, non-membership, insideness and disjointedness, the learning objective can be formulated as

$$\begin{aligned} \min_{\theta, \mathcal{C}} \quad & \sum_{(x_i, l_n) \in \mathcal{D}^+} \mathcal{L}_{\text{membership}}(E_\theta(x_i), \mathbb{B}_{\mathcal{C}(l_n)}) + \sum_{(x_i, l_n) \in \mathcal{D}^-} \mathcal{L}_{\text{non-membership}}(E_\theta(x_i), \mathbb{B}_{\mathcal{C}(l_n)}) \\ & + \lambda \left(\sum_{(v_i, v_j) \in E_h} \mathcal{L}_{\text{inside}}(\mathbb{B}_{\mathcal{C}(l_i)}, \mathbb{B}_{\mathcal{C}(l_j)}) + \sum_{(v_i, v_j) \in E_e} \mathcal{L}_{\text{disjoint}}(\mathbb{B}_{\mathcal{C}(l_i)}, \mathbb{B}_{\mathcal{C}(l_j)}) \right) \end{aligned} \quad (7)$$

The first two terms are losses for positive and negative samples while the last two terms are implication and exclusion constraints, respectively, with λ being the penalty weight of the constraints.

The following corollary shows that our model has a strong inductive bias for preserving consistency.

Corollary 1. *Given a HEX graph G of labels, if the loss terms $\mathcal{L}_{\text{inside}}$ and $\mathcal{L}_{\text{disjoint}}$ are 0, then the learned prediction function is logically consistent.*

Classification via hyperbolic logistic regression A key advantage of our method is that the losses of constraints are compatible with other (margin-based) hyperbolic classifiers such as hyperbolic logistic regression (HLR) [19] and hyperbolic support vector machine (HSVM) [24]. In our experiment we explore HLR, which formulates the *logits* as the distances from an instance to a Poincaré hyperplane of a label. That is, $h(x, l) = d(E_\theta(x), H_C(l))$. $d(\mathbf{p}, H_c)$ has the following closed form:

$$d(\mathbf{p}, H_c) = \sinh^{-1} \left(\frac{2|\langle (-\mathbf{c}) \oplus \mathbf{p}, \mathbf{c} \rangle|}{(1 - \|(-\mathbf{c}) \oplus \mathbf{p}\|^2) \|\mathbf{c}\|} \right) \quad (8)$$

where \oplus is the Möbius addition [19]. The classifier is defined by $f(x) = \{l \mid \sigma(h(x, l)) \geq 0.5, \forall l \in \mathcal{L}\}$ where σ is the sigmoid function. We dub such classifier combined with HMI as HMI+HLR.

4 Evaluation

4.1 Experiment setup

Datasets We consider 12 datasets that have been used for evaluating multi-label prediction methods [11, 8, 10]. These consist of 8 functional genomic datasets [26], 3 image annotation datasets [27, 28], and 1 text classification dataset [29]. All input features are pre-processed in the same way as described by Patel et al. [11]. For all datasets, the implication constraints (label taxonomy) are given. Following Mirzazadeh et al. [15] we add exclusion constraints between sibling nodes whenever this does not create a contradiction (i.e., they share no common descendant nodes). We also explore other strategies for deriving exclusions, but no significant difference was observed (see the supplement for an analysis). Similar to MBM [11] and its baselines, we sample 30% of the implications and exclusions constraints for training the model.

Hyperbolic encoder We adopt a simple hyperbolic linear layer as the instance encoder for all datasets. A single-layer hyperbolic fully-forward linear layer is defined by $f_{\theta=\{\mathbf{W}, \mathbf{b}\}}(\mathbf{x}) = \tanh^\otimes(\mathbf{W} \otimes \mathbf{x} \oplus \mathbf{b})$, with \otimes being Möbius matrix-vector multiplication defined by $M \otimes \mathbf{x} = \tanh \left(\frac{\|M\mathbf{x}\|}{\|\mathbf{x}\|} \tanh^{-1}(\|\mathbf{x}\|) \right) \frac{M\mathbf{x}}{\|M\mathbf{x}\|}$, where $\mathbf{W} \in \mathbb{R}^{n \times d}$ is a trainable matrix and \mathbf{x} is a point $\mathbf{x} \in \mathbb{D}^n$, $M\mathbf{x} \neq 0$. \oplus denotes Möbius addition given by $\mathbf{x} \oplus \mathbf{y} = \frac{(1+2\langle \mathbf{x}, \mathbf{y} \rangle + \|\mathbf{y}\|^2)\mathbf{x} + (1-\|\mathbf{x}\|^2)\mathbf{y}}{1+2\langle \mathbf{x}, \mathbf{y} \rangle + \|\mathbf{x}\|^2\|\mathbf{y}\|^2}$. \tanh^\otimes denotes an Möbius version of pointwise non-linearity given by $\tanh^\otimes(\mathbf{x}) = \exp_0(\tanh(\log_0(\mathbf{x})))$, with \exp_0 and \log_0 being the exponential and logarithmic maps, see [19] for more details.

Baselines We compare our approach with both classical vector-based and state-of-the-art region-based embedding methods. In particular, we consider two vector-based models: 1) The multi-label vector model (MVM) [30], which encodes both inputs and labels as Euclidean vectors; 2) the multi-label hyperbolic model (MHM) used by Chen et al. [13], which represents inputs and labels as hyperbolic points; and two box models: 3) the non-probabilistic box model (BoxE) [31] and 4) the probabilistic multi-label box model (MBM) [11] that encodes both instances and labels as axis-parallel hyper-rectangles. Besides, we compare with 5) hyperbolic logistic regression (HLR) [19] since it also encodes labels as Poincaré hyperplanes (but does not use geometric constraints). Furthermore, we

Table 1: Comparison of performance and consistency on 12 datasets, where underline indicates the best results over embedding-based methods, and **boldface** indicates the best results over all methods. We implemented HMI, HLR and HMI+HLR. Other results are taken from Patel et al. [11]. All metrics are averaged across 10 runs with random seeds (standard deviations are relatively small (in range $[2 \times 10^{-4}, 2.3 \times 10^{-3}]$) and are hence omitted).

Dataset	Metric	Ours		Embeddings				Non-embedding	
		HMI	HMI+HLR	MVM	MHM	BoxE	MBM	HLR	C-HMCNN
ExprFUN	mAP \uparrow	<u>38.53</u>	38.50	37.94	31.90	37.30	38.42	37.98	38.41
	CmAP \uparrow	<u>38.72</u>	38.62	37.41	32.02	37.92	38.67	37.44	38.41
	HCV \downarrow	<u>0.92</u>	1.07	1.97	1.92	4.79	1.87	2.17	0
CellcycleFUN	mAP \uparrow	34.82	<u>34.84</u>	31.61	28.74	31.96	34.61	34.05	34.35
	CmAP \uparrow	34.90	<u>35.00</u>	31.33	28.89	32.70	34.78	34.11	34.35
	HCV \downarrow	<u>1.30</u>	1.32	3.45	1.78	4.02	1.35	2.30	0
DerisiFUN	mAP \uparrow	<u>36.71</u>	<u>36.71</u>	24.16	24.40	26.66	28.71	26.65	28.19
	CmAP \uparrow	<u>36.94</u>	36.89	24.35	24.52	26.96	28.88	26.83	28.19
	HCV \downarrow	<u>0.73</u>	0.87	4.01	0.85	2.27	1.43	2.30	0
SpoFUN	mAP \uparrow	<u>36.47</u>	36.44	24.21	26.57	27.97	29.62	28.29	29.18
	CmAP \uparrow	36.43	<u>36.54</u>	24.55	26.79	28.38	29.78	28.31	29.18
	HCV \downarrow	<u>0.92</u>	1.05	4.73	1.69	2.75	1.53	1.98	0
ExprGO	mAP \uparrow	48.63	48.50	44.97	40.52	46.75	48.45	<u>48.65</u>	48.61
	CmAP \uparrow	<u>48.68</u>	48.61	41.84	40.70	47.28	48.56	48.65	48.61
	HCV \downarrow	1.37	1.45	7.05	5.19	5.74	1.91	1.35	0
CellcycleGO	mAP \uparrow	<u>45.58</u>	45.51	44.19	39.74	43.08	44.93	40.28	<u>45.61</u>
	CmAP \uparrow	<u>45.58</u>	45.53	41.02	39.76	43.79	45.01	40.30	<u>45.61</u>
	HCV \downarrow	1.19	<u>1.12</u>	3.03	2.49	5.06	2.16	3.26	0
DerisiGO	mAP \uparrow	<u>42.31</u>	42.12	41.13	40.10	40.44	42.02	40.33	42.24
	CmAP \uparrow	<u>42.38</u>	42.28	38.21	40.20	40.73	42.12	40.35	42.24
	HCV \downarrow	<u>0.86</u>	0.99	3.46	2.02	3.16	1.13	2.31	0
SpoGO	mAP \uparrow	42.70	<u>42.74</u>	42.20	39.70	40.88	41.74	39.22	<u>42.77</u>
	CmAP \uparrow	42.76	<u>42.77</u>	39.04	39.77	41.27	41.54	39.26	<u>42.77</u>
	HCV \downarrow	<u>0.95</u>	1.20	2.77	1.90	3.89	1.80	2.33	0
Enron	mAP \uparrow	80.43	80.43	73.68	75.62	<u>80.44</u>	80.06	78.87	80.04
	CmAP \uparrow	<u>80.50</u>	80.47	66.87	75.68	<u>80.46</u>	80.05	78.94	80.04
	HCV \downarrow	0	0	2.53	0.36	0.20	0.03	0.04	0
Diatoms	mAP \uparrow	<u>79.19</u>	79.10	72.65	56.86	43.71	79.14	77.90	76.23
	CmAP \uparrow	<u>79.40</u>	79.36	72.18	56.07	45.16	79.23	78.07	76.23
	HCV \downarrow	<u>0.17</u>	0.18	19.20	5.55	6.39	0.34	6.36	0
Imclef07a	mAP \uparrow	<u>90.67</u>	89.60	78.22	65.30	83.71	69.26	88.33	90.26
	CmAP \uparrow	<u>90.89</u>	89.71	77.46	66.01	84.73	69.48	88.45	90.26
	HCV \downarrow	<u>0.20</u>	<u>0.19</u>	22.86	4.75	12.73	2.40	1.77	0
Imclef07d	mAP \uparrow	89.19	89.20	88.59	75.69	87.95	<u>89.56</u>	88.91	89.22
	CmAP \uparrow	90.00	90.02	86.87	76.95	88.93	<u>90.07</u>	87.38	89.22
	HCV \downarrow	<u>0.37</u>	<u>0.36</u>	11.02	7.56	11.93	5.66	6.88	0
Avg. Rank \downarrow	mAP	<u>1.75</u>	2.42	6.33	7.58	5.75	3.5	5.25	3.08
	CmAP	<u>1.58</u>	2.08	7.16	7.41	5.25	3.58	5.41	3.33
	HCV	<u>2.25</u>	2.75	7.42	5.25	7.25	4.25	5.58	1.00

compare with 6) C-HMCNN, a state-of-the-art non-embedding based method that injects hierarchy constraints directly into the loss function without embedding labels. A notable difference is that C-HMCNN needs the full hierarchy constraints as its input. Finally, we also implement HMI+HLR, a combination of our proposed constraints with HLR for an ablation study.

Implementation details We implement HMI, HLR and HMC-HLR using PyTorch [32] and train the models on NVIDIA A100 with 40GB memory. We train HMI, HLR and HMI+HLR using Riemannian Adam [33] optimizer implemented by the Geopt library [34] with a batch size of 4. We also explore some larger batch sizes but it does not yield better results, which is also observed in Wehrmann et al.[14]. We set the dropout rate to 0.6 suggested by [14] to avoid the case that the model overfits the small training sets. We employ an early-stopping strategy with patience 20 to save training time. The results of other baselines are as reported by Patel et al.[11] that we closely follow. The learning rate is searched from $\{1e-4, 5e-4, 1e-3, 5e-3, 1e-2\}$. The penalty weight of the violation is searched from $\{1e-5, 5e-4, 1e-4, 5e-3, 1e-2\}$ and we also show its impact in an ablation. The best dimension per dataset is searched from $\{32, 64, 128, 256\}$, which is one order of magnitude lower than that used by Patel et al. [11] ($\{250, 500, 1000, 1750\}$). All methods have been run 10 times with random seeds and the average results are reported. We omit the standard deviations since they are in a very small range ($[2 \times 10^{-4}, 2.3 \times 10^{-3}]$). Our code is open available at ⁵.

⁵<https://github.com/xiongbo010/HMI>

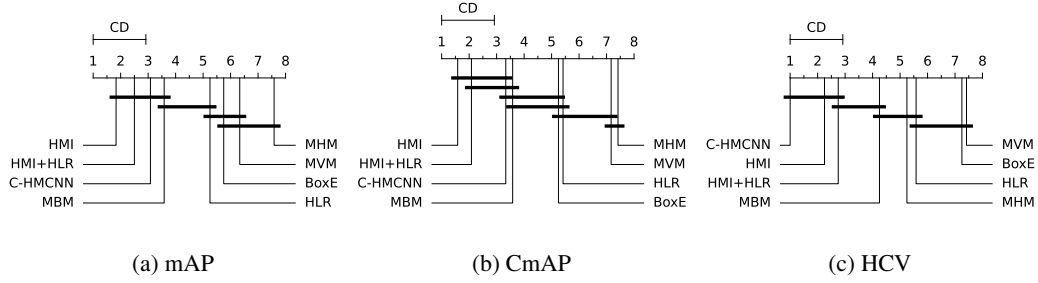


Figure 3: Critical diagrams of the post-hoc Nemenyi test across all 12 datasets.

Evaluation protocols In line with Patel et al. [11], we consider *Mean Average Precision (mAP)*,⁶ which summarizes the information of precisions and recalls with varied thresholds. We also report two metrics that additionally take the constraints into account: 1) *Constrained mAP (CmAP)* is a variant of mAP that replaces the score of each label with the maximum scores of its descendant labels in the hierarchy [11]. 2) *Hierarchy Constraint Violation (HCV)* [11] measures the extent to which the label scores violate the implication constraints regardless of true labels for the instances. HCV is computed as $HCV = \frac{1}{|\mathcal{D}||E_h|} \sum_{k=1}^{|\mathcal{D}|} \sum_{(l_i, l_j) \in E_h} \mathbb{1}(h_i^k - h_j^k > 0)$, where h_i means the prediction score of label l_i . Clearly, a lower value of HCV implies higher consistency in the predictions.

4.2 Main results

As Table 1 shows, our method HMI either achieves the best (7-8/12 datasets) or competitive (4-5/12 datasets) performance (mAP and CmAP) over all compared methods. HMI outperforms all methods w.r.t the average ranking of mAP/CmAP, showcasing the advantages of HMI. We observed that the CmAP is close to mAP, indicating that the model is adhering to the label constraints [11]. In terms of predictive consistency (HCV), HMI consistently achieves the best or the second-best results. Note that C-HMCNN always gets zero HCV because it exploits the complete hierarchy. HMI achieves competitive HCV, despite only using 30% of the hierarchy.

Statistical significance Following Patel et al. [11] and Giunchiglia and Lukasiewicz [8], we test the statistical significance of the performance across all datasets. First, we perform the Friedman test [35] and show that there exists a significant difference w.r.t. all metrics with

p-values $\ll 0.05$. Next, we conduct the post-hoc Nemenyi test to verify the statistical differences of the average ranking. The critical diagram w.r.t the average ranking of mAP/CmAP is shown in Fig. 3, in which the methods that have no significant differences (significance level 0.05) are connected by a horizontal line. As shown in the diagrams, it is clear to conclude that there is a statistically significant difference w.r.t mAPs/CmAPs of HMI and HMI+HLR against MVM, BoxE, MHM, and HLR but not the two strong baselines (MBM and C-HMCNN). We further perform the Wilcoxon test that considers not only the differences in rankings but also the numerical differences in the performance. The Wilcoxon test results show that there is a statistically significant difference between the mAPs/CmAPs of HMI and the two strong baselines with p-value $\ll 0.05$. In terms of HCV, our statistical significance test in Figure 3 and Table 2 shows that HMI and HMI+HLR significantly outperform MVM, BoxE, MHM, HLR, and MBM but not C-HMCNN since it has zero HCV. However, we observed that the predictive performance (mAP, CmAP) is not fully proportional to the HCV, e.g., HMI outperforms C-HMCNN w.r.t. mAP/CmAP on many of the datasets even though C-HMCNN has zero CV.

Table 2: Results of Wilcoxon test over HMI against baselines.

Method	mAP	CmAP	CV
HMI vs C-HMCNN	5.8×10^{-4}	4.4×10^{-4}	5.0×10^{-3}
HMI vs MBM	3.3×10^{-4}	2.4×10^{-4}	4.9×10^{-4}
HMI vs HMI+HLR	2.3×10^{-2}	3.8×10^{-2}	9.7×10^{-1}

⁶https://scikit-learn.org/stable/modules/generated/sklearn.metrics.average_precision_score.html

Classification via hyperbolic logistic regression To validate whether our proposed geometric constraints are able to improve hyperbolic logistic regression (HLR) [19], we implement HMI+HLR, a combination of our proposed constraints with HLR as described in Section 3.3. Table 1 show that HMI+HLR outperforms HLR with statistical confidence, showcasing that HMI is able to improve the predictive performance and consistency of HLR. However, there is no significant difference (with p -value larger than 0.05 in Table 2) between the two variants of our method (HMI and HMI+HLR).

4.3 Ablation studies & parameter sensitivity.

For further ablation, we introduce one additional metric. Exclusion Constraint Violation (ECV) measures, analogous to HCV, the fraction of the exclusion constraints violated by the predictions i.e., $ECV = \frac{1}{|\mathcal{D}||E_e|} \sum_{k=1}^{|\mathcal{D}|} \sum_{(l_i, l_j) \in E_e} \mathbb{1}(f_i^k \wedge f_j^k)$. We introduce this because HCV can be made zero trivially by associating all labels with the same score. Hence, in the ablation study, we will show how the exclusion constraints (the results of ECV) complement HCV and influence the overall performance.

Impact of penalty weight

Table 3 shows the results of HMI on "CellcycleFUN" and "CellcycleGO" dataset. We observed that with different penalty weights, the obtained results are slightly different. Even without penalty ($\lambda = 0$), the model already achieves acceptable results, in particular, it outperforms MVM, MHM, and BoxE, indicating that our hyperbolic model, to some extent, is capable of capturing label hierarchies without any explicit constraints. However, as Table 3 shows, a proper $\lambda = 0.001$, $\lambda = 0.005$ and $\lambda = 0.01$ indeed improves the performance and consistency. Finally, we observed that increasing λ to 0.1, though further improves consistency (HCV and ECV), does not further improve mAP and CmAP. We conjecture that this is because a large λ would encourage the model to "overfit" the given constraints while "underfitting" the classification loss.

Table 3: Impact of violation penalty weight λ on CellcycleFUN and CellcycleGO dataset.

Dataset	Metric	$\lambda = 0.0$	$\lambda = 0.001$	$\lambda = 0.005$	$\lambda = 0.01$	$\lambda = 0.1$
CellcycleFUN	mAP	33.87	34.78	34.82	34.76	32.28
	CmAP	34.03	34.83	34.90	34.85	33.75
	HCV	2.33	1.87	1.30	1.04	0.75
	ECV	4.33	3.77	2.40	1.67	1.35
CellcycleGO	mAP	40.26	41.47	45.58	45.56	41.28
	CmAP	39.87	42.05	45.58	45.60	40.75
	HCV	2.28	1.57	1.19	0.99	0.86
	ECV	3.98	3.27	2.17	1.71	1.34

Impact of implication & exclusion

To study the roles of implication and exclusion. We implemented three variants of HMI by removing either implication or exclusion, or removing both of them. Table 4 depicts the results of these variants. It is clear that both implication and exclusion constraints improve the base model that has no constraints. When implication and exclusion are jointly constrained, the performance is significantly improved again. We also observed that implication and exclusion constraints, to some extent, do complement each other, e.g., by only using implication (resp. exclusion), the model archives lower ECV (resp. HCV). Finally, we observed that even without exclusion, our model still slightly outperforms MBM, showcasing the advantages of hyperbolic space for modeling hierarchies.

Table 4: Impact of implication and exclusion constraints on CellcycleFUN and CellcycleGO dataset.

Dataset	Metric	HMI	w/o implication	w/o exclusion	non constraints
CellcycleFUN	mAP	34.82	34.70	34.74	33.87
	CmAP	34.90	34.75	34.82	34.03
	HCV	1.30	2.34	1.45	2.33
	ECV	2.40	2.67	3.63	4.33
CellcycleGO	mAP	45.58	42.56	44.50	40.26
	CmAP	45.58	42.56	45.31	39.87
	HCV	1.19	2.16	1.73	2.28
	ECV	2.17	3.68	3.07	3.98

Impact of sampling ratio To study whether our method is able to preserve logical constraints from incomplete label constraints we compare the performance of HMI with different ratios for sampling the training constraints. As Figure 4(a) depicts, with zero sampling ratio, our method already achieves acceptable results. We conjecture that this is because some constraints can be learned from the data. However, Figure 4(a) clearly shows that including constraints indeed helps to improve the performance. Making the sampling ratio larger than 30-40% does not lead to a significant

performance gain. We conjecture that this is because certain ratio of training constraints is sufficient for inferring the full set of constraints.

Impact of embedding dimensionality

We study how the choice of dimensionality affects performance. As Figure 4(b) depicts, HMI achieves acceptable results even in a very low dimension ($n \leq 100$). When increasing the dimension an order of magnitude ($n = 1000$), the performance grows only slightly. Note that all reported baselines achieved acceptable results with dimensions in $[500, 1000, 1750]$ (see hyperparameter settings in the Appendix of Patel et al. [11]). We conjecture that the reason we can achieve good performance with fewer dimensions is that the hyperbolic hyperplane is more suitable for representing hierarchical decision boundaries.

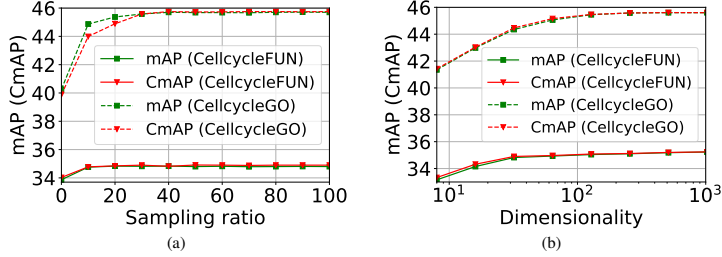


Figure 4: (a) The variation of performance w.r.t the sampling ratio. (b) The variation of performance w.r.t the embedding dimensions.

Comparison with MBM with only implication or without any constraint To faithfully study the advantages of hyperbolic hyperplane on modeling label relations than that of the box model (MBM), we also implement two versions of HMI by considering only (30%) implication constraints and without any constraint (sampling ratio= 0), respectively. Our Wilcoxon test in Table 5 shows that HMI with only implication and HMI without any constraint still outperform their corresponding counterparts of MBM on CmAP and HCV (with p-value < 0.05) while achieving comparable results on mAP (i.e., with better average ranks but without statistical significance, we believe this is because mAP is less sensitive to the constraints than CmAP).

Table 5: Results of Wilcoxon test on HMI against MBM in the settings where only implications are available and without any constraint. — means no statistical difference between the compared methods.

Method	mAP	CmAP	CV
HMI (impl.) vs MBM (impl.)	—	2.4×10^{-4}	1.2×10^{-3}
HMI (no conts.) vs MBM (no conts.)	—	1.3×10^{-2}	6.1×10^{-3}

5 Conclusion

In this paper, we focus on a structured multi-label prediction task whose output is supposed to respect the implication and exclusion constraints. We show that such a problem can be formulated in a hyperbolic Poincaré ball space whose linear decision boundaries (Poincaré hyperplanes) can be interpreted as convex regions. The implication and exclusion constraints are geometrically interpreted as insideness and disjointness, respectively. Experiments on 12 datasets show significant improvements in mean average precision and lower constraint violations, even with an order of magnitude fewer dimensions than baselines.

Acknowledgments

The authors thank the International Max Planck Research School for Intelligent Systems (IMPRS-IS) for supporting Bo Xiong. Bo Xiong is funded by the European Union’s Horizon 2020 research and innovation programme under the Marie Skłodowska-Curie grant agreement No: 860801. Mojtaba Nayyeri is funded by the German Federal Ministry for Economic Affairs and Climate Action under Grant Agreement Number 01MK20008F (Service-Meister). We thank Prof. Martin Keller-Ressel and all anonymous reviewers for providing valuable suggestions that improved the paper.

References

- [1] Jia Deng, Nan Ding, Yangqing Jia, Andrea Frome, Kevin Murphy, Samy Bengio, Yuan Li, Hartmut Neven, and Hartwig Adam. Large-scale object classification using label relation graphs. In *ECCV (1)*, volume 8689 of *Lecture Notes in Computer Science*, pages 48–64. Springer, 2014.
- [2] Jia Deng, Nan Ding, Yangqing Jia, Andrea Frome, Kevin Murphy, Samy Bengio, Yuan Li, Hartmut Neven, and Hartwig Adam. Large-scale object classification using label relation graphs. In *European conference on computer vision*, pages 48–64. Springer, 2014.
- [3] Ranjay Krishna, Yuke Zhu, Oliver Groth, Justin Johnson, Kenji Hata, Joshua Kravitz, Stephanie Chen, Yannis Kalantidis, Li-Jia Li, David A. Shamma, Michael S. Bernstein, and Li Fei-Fei. Visual genome: Connecting language and vision using crowdsourced dense image annotations. *Int. J. Comput. Vis.*, 123(1):32–73, 2017.
- [4] Federico López, Benjamin Heinzerling, and Michael Strube. Fine-grained entity typing in hyperbolic space. In *RepL4NLP@ACL*, pages 169–180. Association for Computational Linguistics, 2019.
- [5] Thi Thuy Duong Vu and Jaehee Jung. Protein function prediction with gene ontology: from traditional to deep learning models. *PeerJ*, 9:e12019, 2021.
- [6] Maxat Kulmanov and Robert Hoehndorf. Deepgoplus: improved protein function prediction from sequence. *Bioinformatics*, 36(2):422–429, 2020.
- [7] Ricardo Cerri, Rodrigo C. Barros, and André Carlos Ponce de Leon Ferreira de Carvalho. Hierarchical multi-label classification using local neural networks. *J. Comput. Syst. Sci.*, 80(1):39–56, 2014.
- [8] Eleonora Giunchiglia and Thomas Lukasiewicz. Coherent hierarchical multi-label classification networks. In *NeurIPS*, 2020.
- [9] Shikhar Murty, Patrick Verga, Luke Vilnis, Irena Radovanovic, and Andrew McCallum. Hierarchical losses and new resources for fine-grained entity typing and linking. In *ACL (1)*, pages 97–109. Association for Computational Linguistics, 2018.
- [10] Jonatas Wehrmann, Ricardo Cerri, and Rodrigo C. Barros. Hierarchical multi-label classification networks. In *ICML*, volume 80 of *Proceedings of Machine Learning Research*, pages 5225–5234. PMLR, 2018.
- [11] Dhruvesh Patel, Pavitra Dangati, Jay-Yoon Lee, Michael Boratko, and Andrew McCallum. Modeling label space interactions in multi-label classification using box embeddings. In *International Conference on Learning Representations*, 2021.
- [12] Wei Bi and James T. Kwok. Multilabel classification on tree- and dag-structured hierarchies. In *ICML*, pages 17–24. Omnipress, 2011.
- [13] Boli Chen, Xin Huang, Lin Xiao, Zixin Cai, and Liping Jing. Hyperbolic interaction model for hierarchical multi-label classification. In *AAAI*, pages 7496–7503. AAAI Press, 2020.
- [14] Jonatas Wehrmann, Ricardo Cerri, and Rodrigo Barros. Hierarchical multi-label classification networks. In *International Conference on Machine Learning*, pages 5075–5084. PMLR, 2018.
- [15] Farzaneh Mirzazadeh, Siamak Ravanbakhsh, Nan Ding, and Dale Schuurmans. Embedding inference for structured multilabel prediction. In *NIPS*, pages 3555–3563, 2015.
- [16] Farzaneh Mirzazadeh. Solving association problems with convex co-embedding. 2017.
- [17] John Venn. I. on the diagrammatic and mechanical representation of propositions and reasonings. *The London, Edinburgh, and Dublin philosophical magazine and journal of science*, 10(59):1–18, 1880.
- [18] Jean Van Heijenoort. Set-theoretic semantics. In *Studies in Logic and the Foundations of Mathematics*, volume 87, pages 183–190. Elsevier, 1977.

- [19] Octavian Ganea, Gary Bécigneul, and Thomas Hofmann. Hyperbolic neural networks. *Advances in neural information processing systems*, 31, 2018.
- [20] Luke Vilnis. Geometric representation learning. *Doctoral dissertations. nr. 2146 University of Massachusetts Amherst*, pages 116–119, 2021.
- [21] Octavian-Eugen Ganea, Gary Bécigneul, and Thomas Hofmann. Hyperbolic entailment cones for learning hierarchical embeddings. In *ICML*, volume 80 of *Proceedings of Machine Learning Research*, pages 1632–1641. PMLR, 2018.
- [22] Ryota Suzuki, Ryusuke Takahama, and Shun Onoda. Hyperbolic disk embeddings for directed acyclic graphs. In *ICML*, volume 97 of *Proceedings of Machine Learning Research*, pages 6066–6075. PMLR, 2019.
- [23] Ben Andrews and Christopher Hopper. *The Ricci flow in Riemannian geometry: a complete proof of the differentiable 1/4-pinching sphere theorem*. springer, 2010.
- [24] Hyunghoon Cho, Benjamin DeMeo, Jian Peng, and Bonnie Berger. Large-margin classification in hyperbolic space. In *The 22nd international conference on artificial intelligence and statistics*, pages 1832–1840. PMLR, 2019.
- [25] Richard V Kadison. The pythagorean theorem: I. the finite case. *Proceedings of the National Academy of Sciences*, 99(7):4178–4184, 2002.
- [26] Amanda Clare. *Machine learning and data mining for yeast functional genomics*. PhD thesis, University of Wales, Aberystwyth, 2003.
- [27] Ivica Dimitrovski, Dragi Kocev, Suzana Loskovska, and Saso Dzeroski. Hierarchical annotation of medical images. *Pattern Recognit.*, 44(10-11):2436–2449, 2011.
- [28] Ivica Dimitrovski, Dragi Kocev, Suzana Loskovska, and Saso Dzeroski. Hierarchical classification of diatom images using ensembles of predictive clustering trees. *Ecol. Informatics*, 7(1):19–29, 2012.
- [29] Bryan Klimt and Yiming Yang. The enron corpus: A new dataset for email classification research. In *ECML*, volume 3201 of *Lecture Notes in Computer Science*, pages 217–226. Springer, 2004.
- [30] Guoyin Wang, Chunyuan Li, Wenlin Wang, Yizhe Zhang, Dinghan Shen, Xinyuan Zhang, Ricardo Henao, and Lawrence Carin. Joint embedding of words and labels for text classification. In *ACL (1)*, pages 2321–2331. Association for Computational Linguistics, 2018.
- [31] Ralph Abboud, İsmail İlkan Ceylan, Thomas Lukasiewicz, and Tommaso Salvatori. Boxe: A box embedding model for knowledge base completion. In *NeurIPS*, 2020.
- [32] Adam Paszke, Sam Gross, Francisco Massa, Adam Lerer, James Bradbury, Gregory Chanan, Trevor Killeen, Zeming Lin, Natalia Gimelshein, Luca Antiga, et al. Pytorch: An imperative style, high-performance deep learning library. *Advances in neural information processing systems*, 32, 2019.
- [33] Gary Bécigneul and Octavian-Eugen Ganea. Riemannian adaptive optimization methods. In *ICLR (Poster)*. OpenReview.net, 2019.
- [34] Max Kochurov, Rasul Karimov, and Serge Kozlukov. Geoopt: Riemannian optimization in pytorch. *CoRR*, abs/2005.02819, 2020.
- [35] Janez Demsar. Statistical comparisons of classifiers over multiple data sets. *J. Mach. Learn. Res.*, 7:1–30, 2006.

A Proof of theorems

Proposition 1. *Given a Poincaré hyperplane H_c where $c \neq 0$, there exists an n -ball $\mathbb{B}_c(o_c, r_c)$ such that $H_c \subset \mathbb{B}_c(o_c, r_c)$, i.e., H_c is a subset of $\mathbb{B}_c(o_c, r_c)$. \mathbb{B}_c is uniquely given by*

$$\mathbb{B}_c^n = \mathbb{B}^n \left(\frac{(1 + \|c\|^2)}{2\|c\|}c, \frac{1 - \|c\|^2}{2\|c\|} \right) \quad (9)$$

Proof. Since c is the center point of the Poincaré hyperplane, the vector \vec{c} must be a normal vector of the tangent space $T_c \mathbb{B}^n$ of \mathbb{B}^n at c . Let q be one of the point that the Poincaré hyperplane and the Poincaré ball intersect at. Then, the radius of $\mathbb{B}_c(o_c, r_c)$, the radius of \mathbb{B}^n , and the distance from the centers of \mathbb{B}^n to the center of $\mathbb{B}_c(o_c, r_c)$ must satisfy the Pythagorean theorem [25], i.e., the three Euclidean distances $d(0, q)$, $d(q, o_c)$ and $d(o_c, 0)$ must satisfy

$$d(0, q)^2 + d(q, o_c)^2 = d(o_c, 0)^2 = (d(0, c) + d(c, o_c))^2. \quad (10)$$

Since we have $d(c, o_c) = d(q, o_c) = r_c$, by solving this quadratic equation, we have $r_c = \frac{1 - \|c\|^2}{2\|c\|}$. Since $o_c = c(1 + \frac{r_c}{d(0, c)})$, we have $o_c = c \frac{(1 + \|c\|^2)}{2\|c\|}$. Thus, $\mathbb{B}_c = \mathbb{B} \left(o_c = c \frac{(1 + \|c\|^2)}{2\|c\|}, r_c = \frac{1 - \|c\|^2}{2\|c\|} \right)$. \square

Proposition 2 (HEX-property). *The classification function f has the HEX property with respect to G if and only if for any constraint in G , the corresponding loss term is 0.*

Proof. Note that the loss term of the constraint being 0 implies that the corresponding constraint is respected. Our loss terms clearly connect the HEX property. That is, for any point $p \in D^n$ and a pair of enclosing n -balls $(\mathbb{B}_w, \mathbb{B}_u)$, $\mathcal{L}_{\text{membership}}(p, \mathbb{B}_w) \geq \mathcal{L}_{\text{membership}}(p, \mathbb{B}_u)$ for all $(\mathbb{B}_w, \mathbb{B}_u)$ where $\mathcal{L}_{\text{inside}}(\mathbb{B}_w, \mathbb{B}_u) = 0$ and $\neg \mathcal{L}_{\text{membership}}(p, \mathbb{B}_w) \vee \neg \mathcal{L}_{\text{membership}}(p, \mathbb{B}_u)$ for all $(\mathbb{B}_w, \mathbb{B}_u)$ where $\mathcal{L}_{\text{disjoint}}(\mathbb{B}_u, \mathbb{B}_w) = 0$. According to the definition of HEX-property, f has the HEX property with respect to G if and only if the corresponding loss term of the corresponding constraint is 0. \square

Corollary 1. *Given a HEX graph G of labels and if the loss of the embeddings is 0, then the learned prediction function is logically consistent with respect to G .*

Proof. Note that the loss terms $\mathcal{L}_{\text{inside}}$, $\mathcal{L}_{\text{disjoint}}$, $\mathcal{L}_{\text{membership}}$, $\mathcal{L}_{\text{non-membership}}$ in Eq.7 are all non-negative. Hence, the loss being 0 implies that all losses are zeros (all constraints are satisfied). According to the definition of consistency, the prediction function is consistent. \square

B Supplementary experiments and details

Datasets and pre-processing The functional genomic datasets (Expr, Spo, Derisi, Cellcycle) are available at ⁷. The image datasets (Imclef07a, Imclef07d, Diatoms) and text dataset (Enron) are all available at ⁸. All licenses of the datasets can be found in the corresponding links and references. The number of labels, types of features, the number of instances vary significantly. The diversity of these datasets makes them suitable for evaluating the multi-label classification task. The input features are pre-processed in the same way as described in [11, 8, 10]. In particular, all categorical features were transformed using one-hot encoding. The missing values were replaced by the mean value (for numeric features) or zero-valued vector (for categorical features). All continuous features were standardized before feeding into the encoder. The labels of the root nodes are removed from training and evaluation.

⁷<https://dtai.cs.kuleuven.be/clus/hmc/datasets/>

⁸http://kt.ijs.si/DragiKocev/PhD/resources/doku.php?id=hmc_classification

Table 6: Statistical information of the datasets used in experiments. Number of features (F), number of classes (L), and number of instances for each dataset split.

Dataset	Domain	Feature	Label	#Label	#Train	#Val	#Test
ExprFUN	Genomics	Continuous	Forest	500	1636	849	1288
CellcycleFUN	Genomics	Continuous	Forest	500	1628	848	1281
DerisiFUN	Genomics	Continuous	Forest	500	1608	842	1275
SpoFUN	Genomics	Continuous	Forest	500	1600	837	1266
ExprGO	Genomics	Continuous	DAG	4132	1636	849	1288
CellcycleGO	Genomics	Continuous	DAG	4126	1625	848	1278
DerisiGO	Genomics	Continuous	DAG	4120	1605	842	1272
SpoGO	Genomics	Continuous	DAG	4120	1597	837	1263
Diatoms	Image	Continuous	Tree	399	1500	565	1054
Imclef07a	Image	Continuous	Tree	97	7000	3000	1006
Imclef07d	Image	Continuous	Tree	47	7000	3000	1006
Enron	Text	Binary	Tree	57	650	338	600

Table 7: The number of exclusion edges derived from the label taxonomy (A) and the label co-occurrence (B).

Dataset	A	B
ExprFun	110958	110941
CellcycleFUN	110959	110942
DerisiFUN	111009	110992
SpoFUN	111008	110991
ExprGO	8305590	8310506
CellcycleGO	8305590	8310506
SpoGO	8257458	8262341
Diatoms	78793	78799
Enron	965	965
ImCLEF07A	4417	4425
ImCLEF07D	979	985

Deriving mutual exclusion In real-world applications, exclusion relations could be annotated by human experts by exploiting domain knowledge. In this paper, we explore various strategies to generate possible exclusion relations: 1) *Deriving exclusion from the label taxonomy*. Following the "exclusive whenever possible" assumption [1], we add mutual exclusion edges between two nodes whenever they do not share any descendant nodes (i.e., it does not create a contradiction). 2) *Deriving exclusion from the label co-occurrence*. We add mutual exclusion edges between two labels whenever there is no instance in the training set simultaneously belonging to them. Clearly, strategy 1 generates all possible exclusion edges entailed by the label taxonomy, while strategy 2 generates exclusion edges that are reflected by the dataset itself. Strategy 1 might create false positive exclusions (i.e., exclusions that violate the label co-occurrence in the datasets), while strategy 2 might suffer from the noisy labeled data (e.g., an instance might be incorrectly or incompletely labeled). However, Table 7 shows that there is no statistical difference between the generated exclusions from these two methods. Hence, we may conclude that the "exclusive whenever possible" assumption almost holds. One common problem of these two methods is that there are many redundant edges generated. To efficiently exploit the constraints, we only generate exclusions between sibling nodes whenever it does not create contradiction [15].